



Response surface methods for membrane humidifier performance

Edward McCarthy*, Sarah Flick, Walter Mérida

Clean Energy Research Centre, University of British Columbia, Vancouver, BC, Canada V6T 1Z4



HIGHLIGHTS

- First report of a designed experiment to evaluate humidifier performance.
- Passive, planar humidifier performance for proton-exchange membrane fuel cells.
- Response surface model is an adequate tool for predicting humidifier performance.

ARTICLE INFO

Article history:

Received 21 July 2012

Received in revised form

10 March 2013

Accepted 1 April 2013

Available online 6 April 2013

Keywords:

Humidifier performance

Design of experiment

Proton-exchange membrane fuel cell

Response surface methodology

ABSTRACT

A designed experiment employing a response surface model was created to evaluate the performance of a passive, planar humidifier intended for the use in PEMFC applications. The performance of this humidifier was analyzed in terms of relative humidity and water transfer rate. For this analysis, a central composite design with four numeric factors was chosen. These four factors were inlet temperature and flow rates on each of two inlet streams. The performance criteria for an acceptable humidifier required air flow from humidifier to fuel cell to be at 80%–100% relative humidity and a temperature between 60 and 80 °C in order to allow for optimal operation of the fuel cell. This experimental design was implemented with a modified fuel cell test station, and humidifiers with two separate membrane types compared. The results of the analysis demonstrate the response surface model to be an adequate tool for evaluating and predicting the tested humidifier's performance. The factors chosen and their interactions show mixed results on humidifier performance.

© 2013 Elsevier B.V. All rights reserved.

1. Introduction

Reactant humidification subsystems contribute significantly to the complexity and cost of polymer electrolyte membrane fuel cell (PEMFC) products. One remaining technical challenge in PEMFC development is the management of water inside the fuel cell stack. A dry membrane can not only become limiting for the overall fuel cell performance; it can also damage the membrane electrode assembly itself. For example, membrane swelling that takes place upon hydration can increase the membrane's dry volume by 10–20% [1,2]. Repetitive volume changes can introduce mechanical stresses which may cause permanent damage or failures, such as membrane rupture [3,4]. Excess liquid water on either the anode or the cathode side of the MEA will decrease the electrode area available for the fuel cell reaction to occur and potentially block the

reactant transport to the active sites, increasing the mass transport losses associated with the reaction. For optimal performance, it is therefore necessary for to maintain the operating conditions, particularly relative humidity, in the fuel cell stack within a narrow range of operating conditions which causes neither dehydration nor flooding.

Numerous methods have been developed to investigate and improve the water management within the fuel cell stack [5–10]. Numerical and experimental analyses for external, gas-to-gas membrane humidifiers with planar geometry have been carried out demonstrating effective performance in PEMFC applications [11–13]. Humidifiers with cylindrical geometry have also been proposed for PEMFC systems [14–17]. However, it is challenging to generalize the results of these experimental or modeling efforts over the broad range of fuel cell operating conditions.

The great modeling challenge of membrane humidifiers is the presence of two-phase flow. This leads to two regions of heat and mass transfer throughout the humidifier: the region of membrane in contact with humidified air, and the region in contact with liquid water. This liquid water distribution is irregular and complicates performance predictions. Kadylak et al. [13] avoid this complication

* Corresponding author. Clean Energy Research Centre, University of British Columbia, 6250 Applied Science Lane, Vancouver, BC, Canada V6T 1Z4. Tel.: +1 604 822 4189; fax: +1 604 822 2403.

E-mail address: mccarthy.edward@gmail.com (E. McCarthy).

Nomenclature	
<i>Symbol and description</i>	
A	membrane area
C	volumetric concentrations of membrane matrix contacting a fluid
D	vapor transfer coefficient
G	vapor molar mass
ṁ	mass transport
M	membrane equivalent weight
n	number of factors
k	order of a response
R ^x	resolution of a design (<i>x</i> in Latin numerals)
t	membrane thickness
T	temperature
x	factor levels in a regression equation
<i>Greek symbols</i>	
α	location of star points
β	regression coefficients
<i>Subscripts</i>	
λ	water content
ρ	membrane density
ϕ	relative humidity
<i>Abbreviations</i>	
PEMFC	proton exchange membrane fuel cell
MEA	membrane electrode assembly
DoE	design of experiment
WTR	water transport rate
RSM	response surface methods
CCD	central composite design

by modeling only with conditions resulting in non-condensing flows, either isothermal or low humidity. Work such as that by Chen et al. [14], which models heat and mass transfer between liquid and dry gas streams through a Nafion membrane, illustrates the difficulty of analytical models in modeling the complex phenomena present in membrane humidifiers. Their equation for water transport,

$$\dot{m}_{1,v,tr} = D_w \frac{C_2 - C_1}{t_m} G_v A \quad (1)$$

contains three terms dependent on water content and phase on either side of the membrane. C_x , the volumetric concentrations of the membrane matrix in contact with air ($x = 1$) or water ($x = 2$), is given by

$$C_x = \frac{\rho_{m,dry}}{M_{m,dry}} \lambda_x \quad (2)$$

Chen et al. demonstrate that λ_1 can be obtained from a curve fit depending on ϕ_1 and indicate that λ_2 , which can take any value from 14 to 22, must be determined based on experimental data. Finally,

$$D_w = D_\lambda e^{E_0 \left(\frac{1}{303} - \frac{1}{T} \right)} \quad (3)$$

where D_λ has a piecewise-linear equation depending on the membrane water content λ_m , in turn dependent on ϕ_2 , approximated by Chen et al. as the arithmetic mean of dry and wet side relative humidities.

λ_x , λ_m , and T are all local quantities, subject to significant change between inlet and outlet, or from layer to layer for a planar humidifier such as the ones in this paper, for a humidifier operating under fuel cell conditions. An accurate calculation of heat and mass transport across the full range of operating conditions must take into account the variation of these quantities, as well as the two-phase nature of the flow. The computational expense of modeling this for a full-scale humidifier is prohibitive; work to date has focused on modeling simplified humidifiers under simplified conditions [11–17]. The present work

addresses this limitation in the existing literature with an empirical model.

A reliable approach for developing an empirical model of humidifier performance is provided by the design of experiments (DoE) methods. Designed experiments have the ability to cover a full range of operating conditions and assess the effects of interactions between chosen factors. These methods are of particular use in complex systems affected by numerous factors, and are commonly used in the practice of chemical engineering. Recently, the literature shows a growing body of work using DoE methods for the study of PEM fuel cells, which are themselves complex systems [18–24]. A broad range of DoE techniques have been used in PEMFC research [21,24–30], but only Cave and Mérida have used a designed experiment – a 2^k full factorial – in characterizing humidifiers [31].

In this paper, the DoE method is applied to the study of a planar membrane humidifier intended for use on the cathode side of a 10 kW PEMFC system. A discussion of the humidifier system is used to select an appropriate design and factors. The operating range and desired outputs are based on the operating range of a PEMFC. The resulting designed experiment is executed and data analysis performed to produce a response surface for a test humidifier with respect to the humidification requirements of a PEMFC. The results of this study are discussed with respect to previous research.

2. Creating empirical models using response surface methodology

Response surface methods and analysis, also known as response surface methodology (RSM), is a selection of statistical and mathematical techniques used to develop, improve and optimize processes [32,33]. In most cases, multiple regression is used to develop the empirical models. A simple, general equation for a second-order response surface model describes a response y in terms of two variables x_1, x_2 :

$$y = \beta_0 + \beta_1 x_1 + \beta_2 x_2 + \beta_{11} x_1^2 + \beta_{22} x_2^2 + \beta_{12} x_1 x_2 + \epsilon. \quad (4)$$

The parameters β_j are regression coefficients that will be determined during the model fitting, ϵ represents the statistical

error, which is assumed to have a normal and independent distribution with mean zero and variance σ^2 , ($\varepsilon \sim NID(0, \sigma^2)$). The variables, also called factors, used in the regression model can be quantitative (measurable on a scale) or qualitative. Qualitative factors may be assigned numerical levels if necessary. The regression coefficients are fit based on experimental data collected in experiments designed so as to maximize the value of the information gathered for curve fitting, while minimizing experimental expense.

In order to fit the regression coefficients to describe the desired response function based on the measured data and observations, the method of least squares is commonly used. Sophisticated models may also be fitted with the aid of statistics software. After the initial fit a careful statistical analysis of the empirical model has to be conducted to determine the validity and usefulness of the model. Once the regression parameters have been determined it is necessary to assess the significance of the regression using either hypothesis testing or analysis of variance (ANOVA) testing, which was employed in this work. Confidence intervals for regression coefficients and mean responses can also be useful to further analyze the model fit.

Once the model is fitted adequacy checking via a residual analysis and lack of fit testing is required to assure a relevant approximation of the empirical model to the physical underlying system. It is important that none of the least squares regression assumptions should have been violated [32].

3. Selection of the design parameters

The first step of a designed experiment is to select and quantify the relevant factors from a pool of operating parameters. Typical planar membrane humidifiers have four ports as illustrated in Fig. 1. For consistency the flows at each inlet and outlet are numbered according the order in which they are encountered by the intake oxidant: the dry inlet (1), the dry outlet (2), the wet inlet (3), and the wet outlet (4).

The states at the outlets are completely determined by the state at the inlets and the heat and water exchange that takes place over the length of the humidifier. Humidifier performance can be broadly defined as the efficacy of the humidifier at transferring water from the wet stream to the dry stream during operation. Quantifying this efficacy, however, requires some consideration. In the present work we focus on metrics that are relevant to humidifier operation in a PEM fuel cell system. Adequate fuel cell inlet humidification requires stream 2 relative humidity (ϕ_2) to be in the range of 80%–100% and a temperature between 60 and 80 °C in order to prevent drying effects while maintaining acceptable performance [34].

Relative humidity is an awkward choice when describing humidifier performance, as the relative humidity of stream 2 depends

not only on the water transferred, but also the temperature, pressure, and mass flow of air at the humidifier outlet. Despite its limitations, the relative humidity elegantly combines two separate aspects of humidifier performance: the water transfer and heat transfer rates. The raw metric of humidifier performance is the “water transfer rate” (WTR), the absolute rate in g min⁻¹ at which water moves across the humidifier membrane from wet gas to dry gas. This metric, out of context, provides little to no information about humidifier efficacy, as the same WTR in two differently sized humidifiers with different flow rates could result in very divergent stream 2 conditions.

In addition to transferring water, the humidifier transfers heat from the hot stream to the cooler stream. The measured relative humidity, as defined in Equation (1) combines two controlled experimental parameters, P_2 and \dot{m}_{air} , and two key humidifier outputs, WTR and T_2 , into one metric.

$$\phi_2 = f(WTR, T_2, P_2, \dot{m}_{air}) \quad (5)$$

As mentioned above, however, relative humidity provides a range of desirable operation for PEM fuel cell performance. As long as a humidifier can perform robustly within that desirable range, the performance is acceptable. Humidifiers meeting the relative humidity criterion can be ranked by WTR, or by economic factors such as cost and size.

3.1. Factors

The independent factors affecting humidifier performance are the factors at the inlets. In a passive humidifier, these inlet factors at streams 1 and 3 can be controlled and determine the states at streams 2 and 4. These factors are the dry air flow rate, the dry bulb temperature, the water content, and the pressure for each of the two inlets. The parameters considered in the factor selection for the experiments are chosen from the flow parameters. Each of these four parameters – humidity, temperature, flow rate, and pressure – can take a distinct value in stream 1 and stream 3 at each inlet. This means that there are eight distinct parameters in humidifier operation. These are outlined in Table 1, and can be seen schematically below in Fig. 2.

3.2. Factor values

The next step in the experimental design is to determine the “levels”, or experimental settings, of the factors in the experiment. The factors used in this study, and their levels in terms of real values, are summarized in Table 2. Each factor will be coded into a value normalized around 0, usually ranging from -1 to +1. Convention in DoE implementation is to assign a separate, alphabetic factor name to the coded level of each factor. This serves to distinguish the coded factor from the real factor. The usual nomenclature refers to the real value, rather than the coded level of the factor and is described below. Table 2 also presents the names used for each of these factors in the experimental design.

3.3. Design selection

The selection of the design used in this work is based on the objective to maximize efficiency of the humidifier. As there are four numeric factors present, the following assumptions (I–III) and considerations (IV–VI) were taken into account.

- I. The nature of the system and the non-linear dependence of the saturation pressure $p_{sat}(T)$ of water vapor in air made a linear response unlikely.

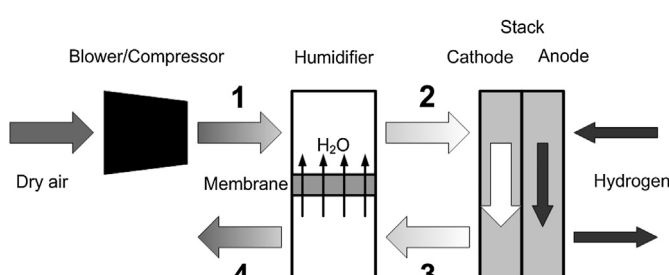


Fig. 1. Schematic of planar cathode humidification system illustrating the flow naming conventions.

Table 1
Factor selection for design of experiments.

Parameter	Stream 1	Stream 3
Relative Humidity	Eliminated from the design due to small variation between systems; $\phi_1 = 0\%$ at T_1	Eliminated from the design due to small variation between systems; $\phi_2 = 100\%$ at T_3
Temperature	Depending on system manufacturer and application, the temperature can range from atmospheric to a temperature that is higher than the stack's during steady operation. Factor: $T_{1\min} = 25^\circ\text{C}$ and $T_{1\max} = 110^\circ\text{C}$	Variation in T_3 at $\phi_2 = 100\%$ will have a significant effect on the humidity ratio in stream 3. Factor: $T_{3\min} = 60^\circ\text{C}$ and $T_{3\max} = 80^\circ\text{C}$
Flow rate	Set by the fuel cell stoichiometry and power demand, can be varied independently. Factor: $Q_{1\min}$ and $Q_{1\max}$ set between 50 SLPM and 250 SLPM	Set by the fuel cell stoichiometry and power demand, can be varied independently. Factor: $Q_{3\min}$ and $Q_{3\max}$ set between 50 SLPM and 250 SLPM
Pressure	P_1 , in this study, was treated as the outlet pressure a humidifier for automotive applications. In this case, P_1 was set at 170 kPag (1.7 barg)	There is a pressure drop through the cathode, but otherwise no independent control of P_3 in a passive humidifier system; P_3 is set by P_1 , with $P_3 < P_1$; in this case P_3 is 140 kPag (1.4 barg)

- II. Previous work suggested the existence of second-order interactions.
- III. The existence of significant third- (or higher-) order interactions over and above the second-order interactions was assumed to be unlikely, in order to increase efficiency of the experimental design. In DoE practice, these higher-order interactions are exceedingly rare [33].
- IV. The purpose of these experiments was to model interactions and response across the humidifiers' operating range, as defined in the factor selection step.
- V. Humidifiers are designed to operate more within their operating range than at the edges.
- VI. Testing expense is to be minimized.

These assumptions and considerations led to the decision to use a response surface design for humidifier characterization. Response surface methodology (RSM) is a class of DoE intended to provide a continuous estimate of the measured response across the range of possible factor combinations. The graphical result of an RSM experiment is a surface in n -dimensional space that describes the response in terms of n considered factors, and includes the effects of their interactions. An estimate of variance across the response surface is also provided through RSM techniques. These response surface methods have resolution R^V , meaning that no response of

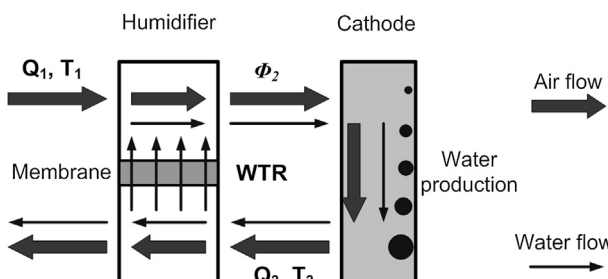


Fig. 2. Schematic of factor locations.

Table 2
Selection of factor values.

Factor	Factor name	Range of values
Q_1	A	50–250 SLPM
Q_3	B	50–250 SLPM
T_1	C	$25^\circ\text{C} \leq T_1 \leq 110^\circ\text{C}$
T_3	D	$\phi_1 = 0\%$ $60^\circ\text{C} \leq T_3 \leq 80^\circ\text{C}$ $\phi_3 = 100\%$

order k is aliased with any response of order less than $5 - k$. All first and second order responses are independent of one another.

The experimental design chosen was a central composite design (CCD), a design which sees widespread use in DoE applications [32]. The most significant factor in the choice of this design was the design's use of 5 levels of each factor, allowing a very good estimate of curvature. This was important because the system was expected to display non-linear behaviors.

One benefit of the CCD, excepting a "rectangular" variant of CCD design which uses only 3 levels of each factor, is that it avoids continued experimentation at the extreme values being tested. This can be of significant benefit because testing these points may be problematic or undesirable. These points may be difficult to reach, maintain, or control; they may increase the potential for equipment damage; or they may simply not be common operating conditions.

This experiment used a CCD, consisting of six center points, star points at $\alpha = \pm\sqrt{2}$ in coded values, and a two-level full factorial design. The design uses four numeric factors while the pressures at streams 1 and 3 were held constant. The numeric factors and factor values for the DoE are summarized in Table 3.

4. Experimental

4.1. Test apparatus

The two humidifiers used in this experiment were dPoint's Px3-46 type. The Px3-46 humidifier plate is 160 mm long, 55.7 mm wide, and has a depth of 0.85 mm. A Px3-46 is built such that the total height of plates and membrane is 46 mm. It may be operated at flow rates ranging from 50 SLPM to 250 SLPM.

Two different membranes were tested in the humidifier; designated here as membranes M and N. Membrane M is a porous polymer membrane, while membrane N is an ionic perfluorinated composite membrane. Humidifiers with membrane N also used a porous woven support layer against the membrane on the wet, lower pressure side. One of the Px3-46s was made with membrane M while the other one used membrane N. These membranes differ in both physical and chemical characteristics. The same designed experiment is used to produce an empirical model for each membrane, in order to demonstrate the applicability of this method to humidifiers using diverse materials.

Table 3
Final values for design of experiments.

Numeric factors	Factor values				
	$-\alpha$	-1	0	1	α
A: Q_1 , SLPM	50	79.3	150	220.7	250
B: Q_3 , SLPM	50	79.3	150	220.7	250
C: T_1 , $^\circ\text{C}$	25	37.3	67.5	97.7	110
D: T_3 , $^\circ\text{C}$	60	62.9	70	77.1	80
Constant	Constant level				
E: Pressure, kPa	$P_1 = 170$, $P_3 = 140$				

All testing was carried out on a modified Greenlight GenIV fuel cell test station. This test station and its packaged software were originally designed to deliver and control cathode and anode reactants directly to a fuel cell mounted on the test bench. The test stand was modified to deliver and control only humidified air flows. The air supplied as stream 1 was compressed air with $\phi_1 \approx 0\%$ controlled by a Teledyne HFC-303 mass flow controller with a reported full scale accuracy of $\pm 1\%$ for the relevant flow rates. To humidify stream 3 a calibrated customized spray injector system was used. Type-K thermocouples were used as temperature sensors and temperature control was achieved using heater blocks integrated to the spray injector. A flow diagram illustrating the test apparatus is shown in Fig. 3.

In order to measure the water transfer across the humidifier a condensing water balance was employed at the outlet of stream 2. The exhaust of stream 2 is cooled down to a temperature of $12^\circ\text{C} \pm 2^\circ\text{C}$ and the amount of liquid water produced is measured. Therefore stream 2 is directed through an indirect heat exchanger supplied with cold building water. Cooled air and supersaturated water are then entered in a large condensation chamber in which the condensed water droplets are collected and lead to the water balance.

An experimental protocol was developed and the testing order randomized to eliminate operational bias. All tests were conducted under steady state conditions under the same atmospheric conditions in the laboratory. Measurements were taken over 10 min intervals, with Greenlight's FC Analytics software taking a log point of all data input at intervals of 10 s. This allowed the use of 600 data points for averaging the steady state conditions. After each test point, the factor values on the software were set to the following test point.

4.2. Statistical model

The experimental matrix and post-experimental analysis employing analysis of variance tables were conducted with the aid of Design Expert 7 software. The saturation pressures were calculated using the Goff–Gratch equation. The resulting equations, in terms of their coded values, are shown in Table 4. The size of the

Table 4
Model equations in coded values.

Membrane M ϕ_2	Membrane M WTR	Membrane N ϕ_2	Membrane N WTR
$\text{Ln}(\phi_2) = -0.71$	$\text{Sqr}(WTR) = 2.75$	$\text{Ln}(\phi_2) = -0.65$	$\text{Sqr}(WTR) = 2.9$
$-0.21 * A$	$0.42 * A$	$-0.23 * A$	$0.44 * A$
$0.11 * B$	$0.18 * B$	$0.071 * B$	$0.16 * B$
$-0.55 * C$	$-0.58 * C$	$-0.49 * C$	$-0.41 * C$
$0.073 * D$	$0.5 * D$	$0.069 * D$	$0.5 * D$
$0.1 * E$	$-0.5 * E$	$0.042 * E$	$-0.62 * E$
$0.018 * A \times B$	$0.066 * A \times B$	$0.048 * A \times B$	$0.1 * A \times B$
$-0.28 * A \times C$	$-0.17 * A \times C$	$-0.31 * A \times C$	$-0.17 * A \times C$
$4.34E-03 * A \times D$	$0.033 * A \times D$	$0.017 * A \times D$	$0.049 * A \times D$
$0.14 * A \times E$	$0.095 * A \times E$	$0.082 * A \times E$	$0.035 * A \times E$
$0.12 * B \times C$	$-0.057 * B \times C$	$0.14 * B \times C$	$-0.034 * B \times C$
$-0.03 * B \times D$	$0.02 * B \times D$	$-0.011 * B \times D$	$0.014 * B \times D$
$7.93E-03 * B \times E$	$0.013 * B \times E$	$-0.01 * B \times E$	$-3.15E-03 * B \times E$
$0.055 * C \times D$	$-0.13 * C \times D$	$0.037 * C \times D$	$-0.11 * C \times D$
$0.11 * C \times E$	$0.29 * C \times E$	$0.072 * C \times E$	$0.19 * C \times E$
$-0.014 * D \times E$	$-0.13 * D \times E$	$-3.49E-03 * D \times E$	$-0.13 * D \times E$
	-0.16	A^2	$-0.14 * A^2$
	-0.038	B^2	$-0.054 * B^2$
	0.23	C^2	$0.18 * C^2$
	0.12	D^2	$0.092 * D^2$

coefficients of the coded values indicates the importance of the corresponding factors, and the sign indicates whether the factor is positive or negative. These equations are transformed to eliminate kurtosis in the results and to provide the best fit; the transforms are noted in the equations. All equations have p -values of under 0.0001, implying high significance; there is under a 0.01% chance that these models are noise.

5. Results and discussion

The model produced through this set of experiments is a parametric equation for each of ϕ_2 and WTR including both first- and second-order factors, for a total of four first-order factors and eight second-order factors. For the purposes of comparison, the results are analyzed in terms of the two performance metrics discussed in Section 3: the relative humidity of stream 2 and the water transfer

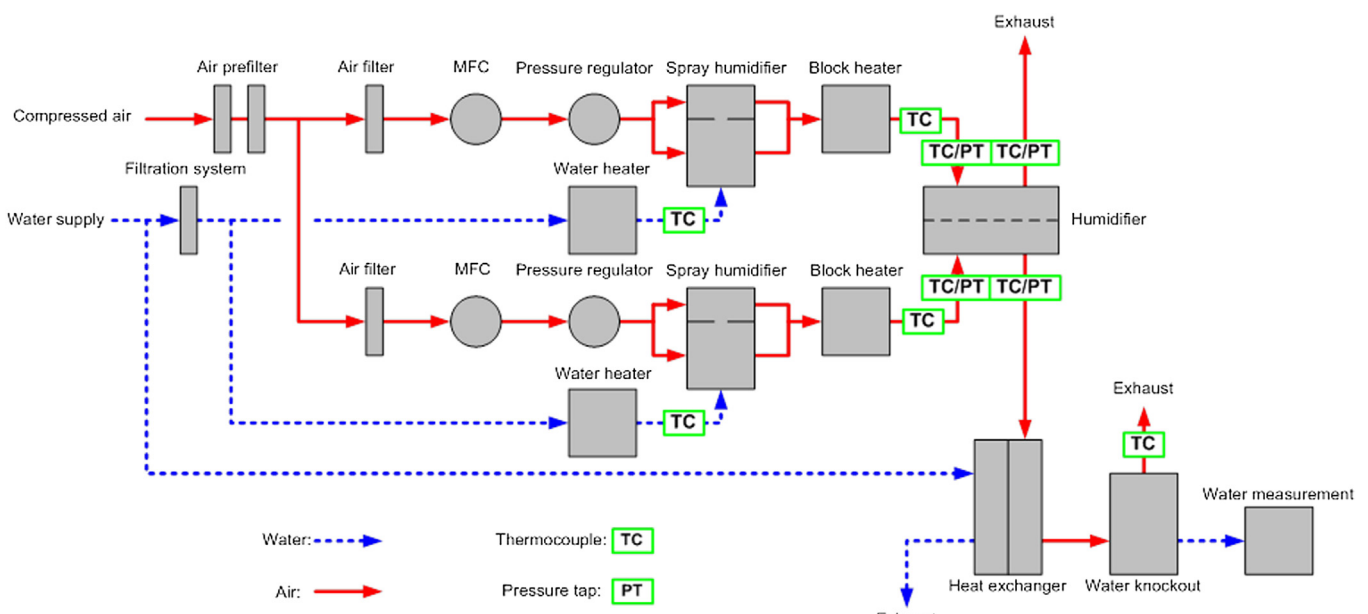


Fig. 3. Schematic of test apparatus.

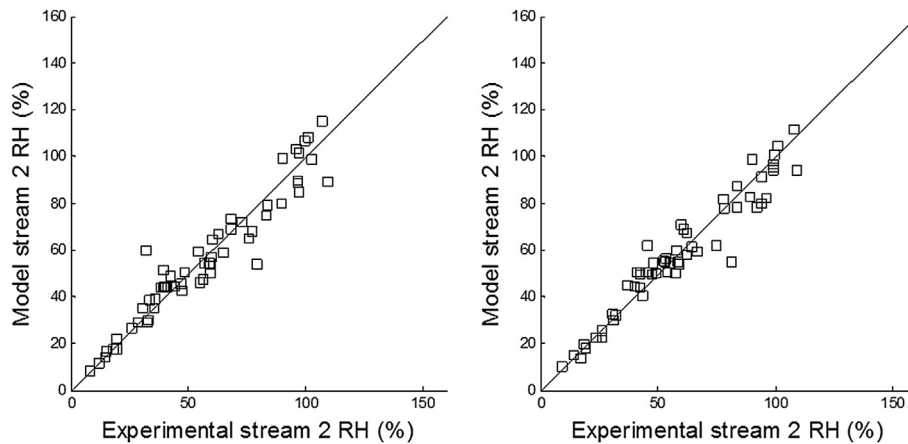


Fig. 4. Error plots for membrane M and membrane N for ϕ_2 .

rate. The data used to produce the response surfaces for each of the metrics investigated here are based on direct physical measurements of temperature and pressure and on the assumptions of mass conservation through the humidifier as well as of full saturation of the outlet stream of the water balance. Standard psychrometric relations were used to calculate the set of data for the six metrics at each experimental point from these initial measurements. As such, the data used to produce the response surfaces are thermodynamically consistent between metrics. Each set of data, however, is subject to a separate statistical analysis to produce its response surface model. The relations used to produce the data are not linear; the stream 2 relative humidity is subject to a natural logarithm transform, and the water transfer rate to a square root transform. These transforms were chosen based on information from the Box–Cox plot for each set of results. This transformed data is subjected to a least squares analysis. Following these operations, thermodynamic consistency is no longer maintained between the two response surfaces produced. The implication of this is the models produced for ϕ_2 and WTR will not correlate directly onto one another using the standard relationships between ϕ_2 and WTR.

Inspection of the results of the least squares analysis shows that both of these metrics had a good fit to the model produced for them. Fig. 4 displays modeled versus measured ϕ_2 and Fig. 5 shows the error between modeled and measured WTR for both membrane M and N. The error plots show the difference between the experimental results obtained and the results predicted by the response

surface at each given point. The normal plots, Figs. 6 and 7, show the fit of the residuals to the normal distribution. In both the error and the normal plots, for an ideal model the points would line up along the diagonal. In the case of the error plot, significant differences indicate a deficiency of the model in predicting those points; in the case of the normal plot, a significant trend of points away from the diagonal indicates that the errors are not normally distributed. This tends to imply either that a different transform is needed, or that there is a significant source of error beyond random error which is not being accounted for. In these plots, the only element of slight concern is the slight skewness of the Membrane M error plot for ϕ_2 ; the results are fairly close to the normal.

The model results are shown in 2-dimensional compound plots (Figs. 8–11), a compact way to show multidimensional data. In order to allow a visualization of all four numeric factors and the response, each plot consists of twelve contour subplots. One diagonal of the plot is taken up by subplotted boxes containing a factor name and scale. These scales are projected vertically and horizontally to provide the scales for each of the subplots. In each two-dimensional contour plot the factors not involved are maintained at a constant level. It can be noted that the twelve subplots are in fact six pairs of identical plots, only with the axes reversed. Scales in ϕ go to 150%; this reflects that the total water content is up to 1.5 times the saturation limit.

In addition to providing a predictive model for performance, the response surface analysis results allow an estimate of the effects of

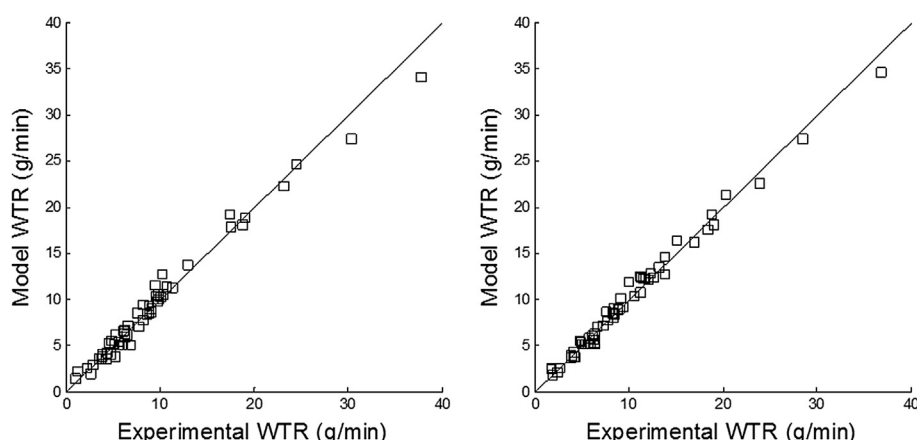


Fig. 5. Error plots for membrane M and membrane N for WTR.

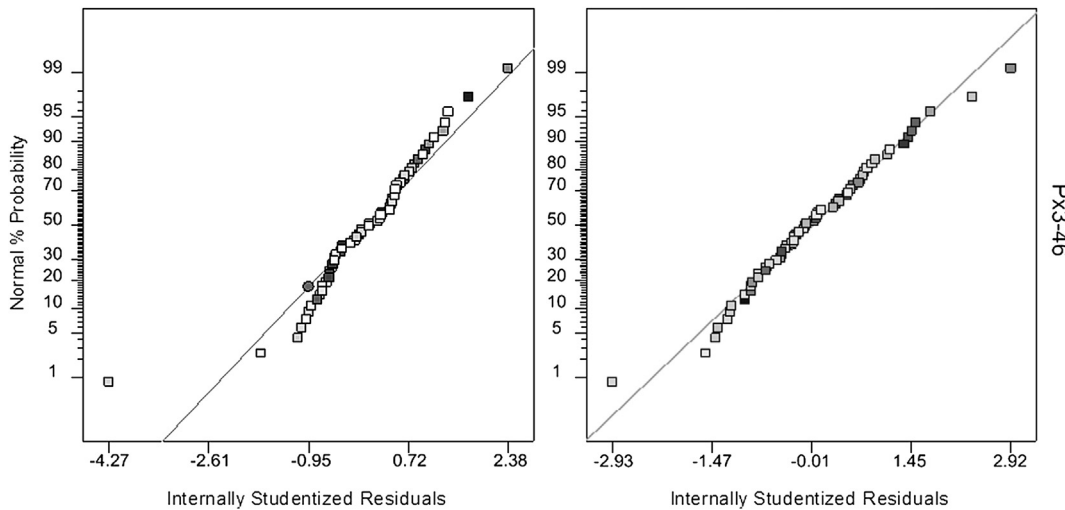


Fig. 6. Normal plots of residuals for membrane M and membrane N for ϕ_2 .

main factors and of significant interactions. It is important to note that these main factors and significant interactions match for membranes M and N. This is expected. When using models such as (1) to assess mass transport, t_m and D_w are membrane-dependent, as are the terms $\rho_{m,dry}$ and $M_{m,dry}$ from (2). Adjusting these terms for each membrane changes the magnitudes of the main effects and interactions, but not the general transport behavior of the humidifier.

Stream 1 flow rate is a conflicting response. High stream 1 flow rates result in improved water transport as water is more quickly and efficiently convected away from the membrane surface. Higher stream 1 flow rate, however, implies more water needed to reach the desired ϕ_2 of 80%–100%. As such, higher stream 1 flow rates lower the efficacy of humidification for the fuel cell application.

The system appears quite robust to changes in stream 3 flow rate. Increased stream 3 flow results in marginal increase in ϕ_2 and in WTR. This suggests that the rate of water transport is limited by transport processes in the membrane, and implies that improved membrane technology will provide significant opportunities for humidifier improvement.

Increasing T_1 has a strong negative effect on performance. This negative effect is the most consistent result of this study. The reasons for this effect are discussed by Romero and Mérida in Ref. [35]. The high T_1 initially increases the evaporation of water from the membrane surface, to the point that the rate of transport from the surface is higher than that at which water is conducted through the membrane. This causes a drying of the membrane layer adjacent to the dry stream. This dry membrane subsequently acts as a barrier to further water transport, resulting in the significant decrease in water transport observed with increases in T_1 . As this work considers only steady state measurements, the likely transient increase in water transport at the beginning of this process is not seen.

The effect of T_3 is combined with the effect of increasing water content in stream 3 as the dew point temperature is raised, since $\phi_3 = 100\%$. This has a strong positive effect on absolute performance as judged by WTR caused by the effects of more water supplied to the wet side of the membrane. The effect on ϕ_2 is mixed. The small values seen in the ϕ_2 effect are caused by the dependence of the ϕ_2 measurement on the dry bulb temperature of the stream as well as the wet bulb temperature. A higher value of T_3 has a heating effect

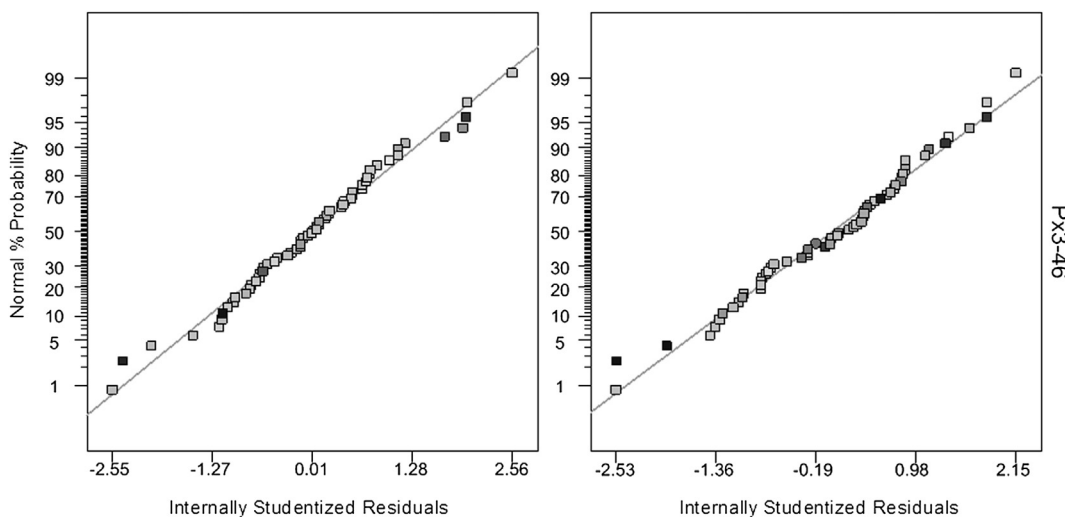


Fig. 7. Normal plots of residuals for membrane M and membrane N.

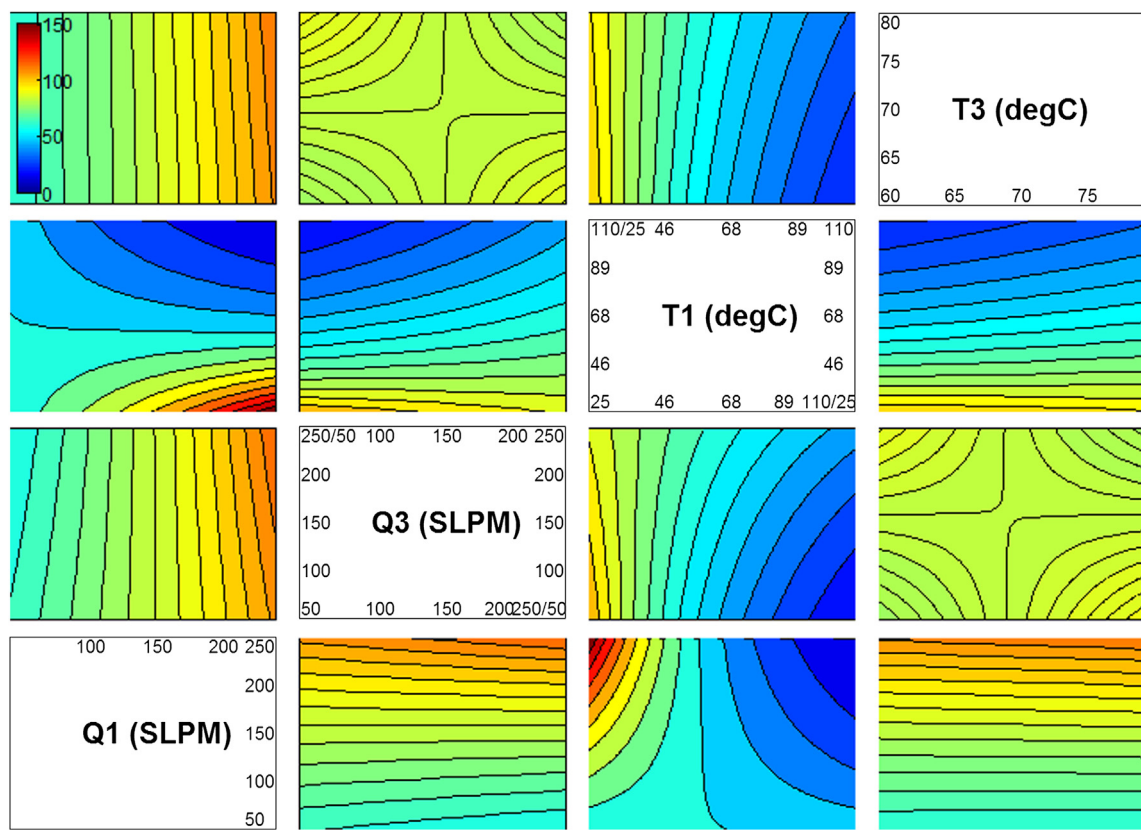


Fig. 8. Plot for membrane M, ϕ_2 , scale in % ϕ .

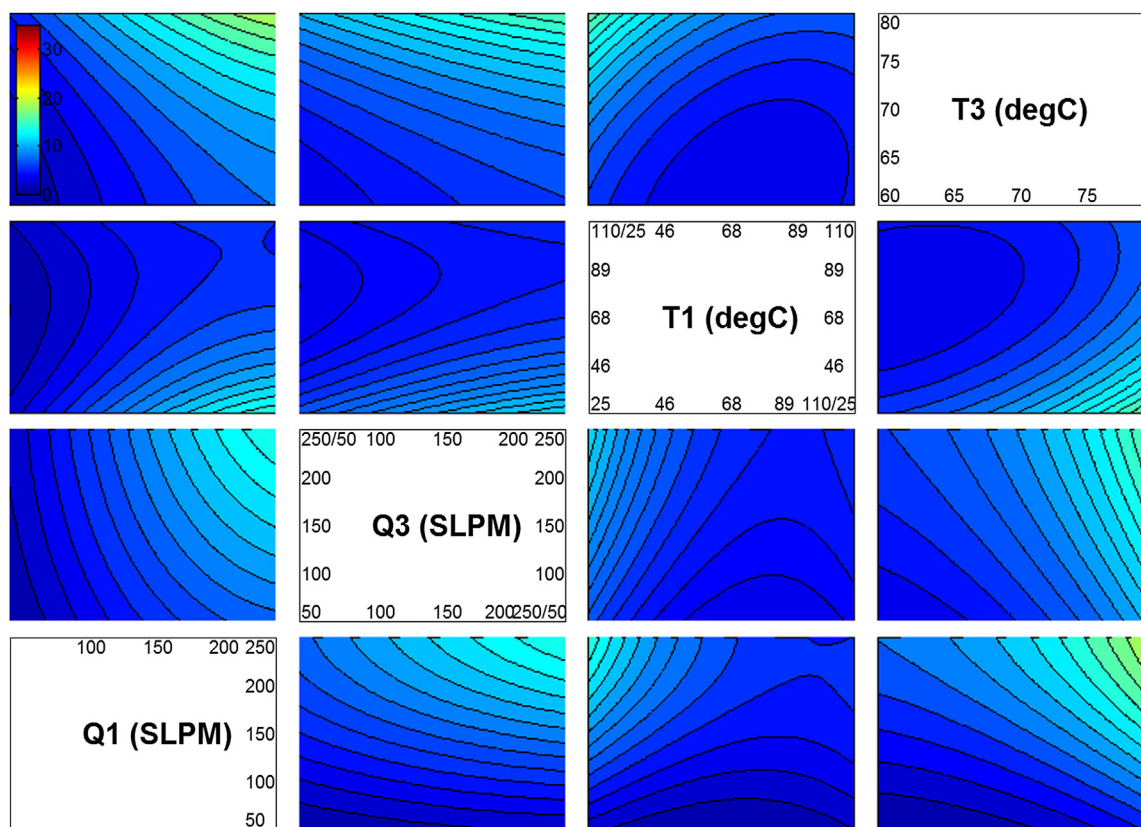


Fig. 9. Plot for membrane M, WTR, scale in g min^{-1} .

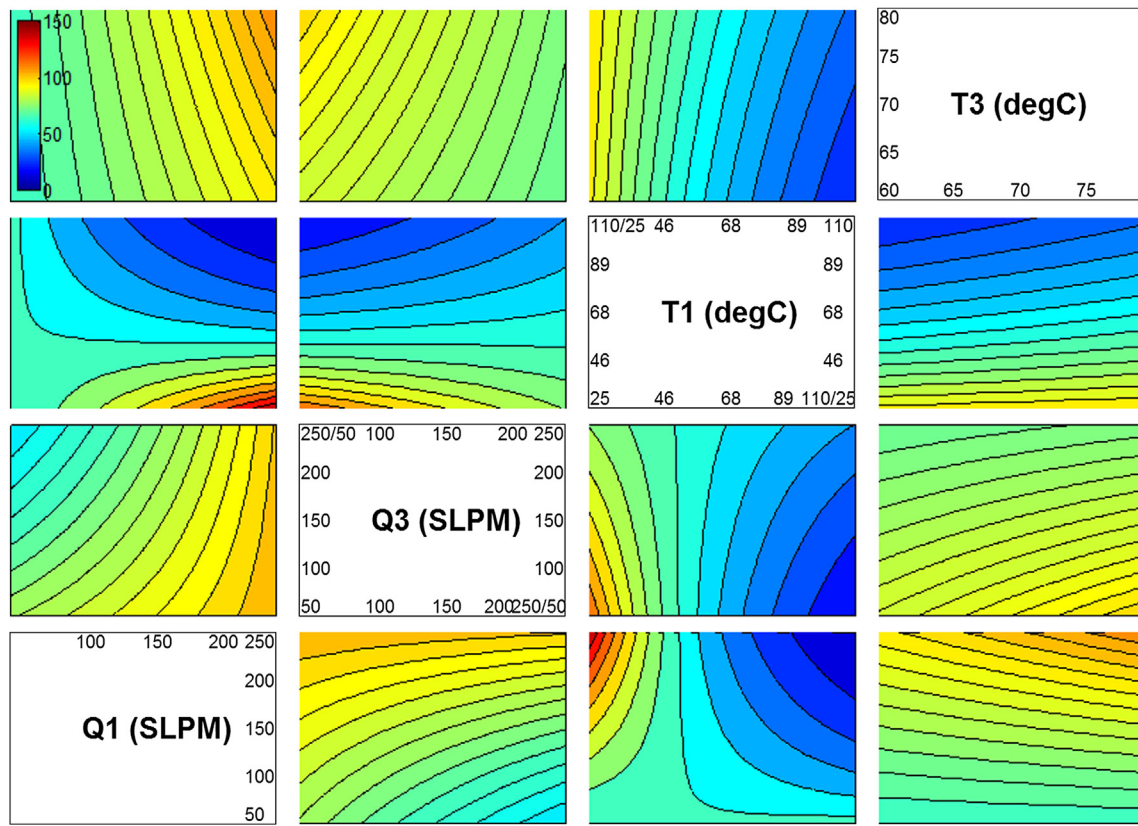


Fig. 10. Plot for membrane N, stream 2 ϕ , scale in % ϕ .

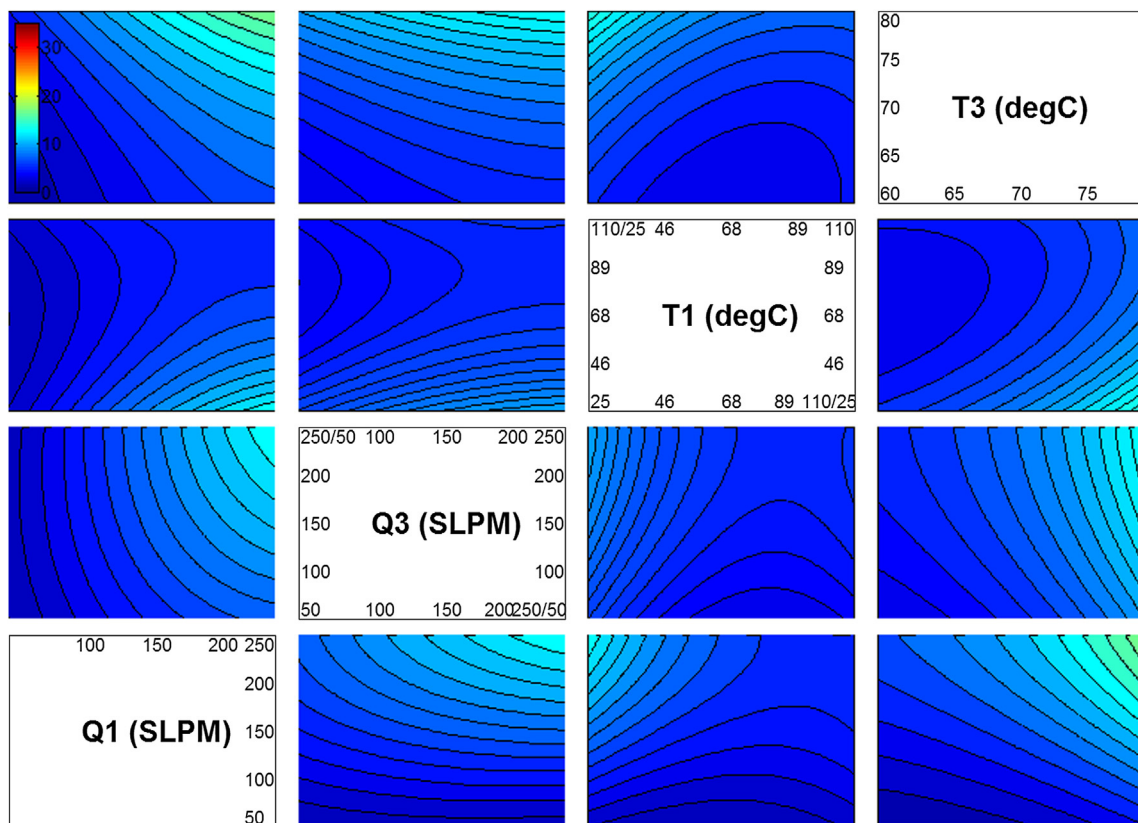


Fig. 11. Plot for membrane N, WTR, scale in g min^{-1} .

on stream 2, raising its saturation pressure and thereby creating a demand for greater water transport to increase ϕ_2 .

6. Conclusions

The performance of a passive, planar humidifier intended for the humidification of reactant gases in a PEMFC was modeled using DoE methods. The performance of the humidifier was evaluated in terms of ϕ_2 and in terms of WTR. The desired value of ϕ_2 was set to be between 80 and 100% for relevance in fuel cell applications. Four numeric factors and one constant factor were incorporated in a central composite design. A RSM model was created in order to meet the system's specific requirements and allow for evaluation of second order interactions of the factors. An experimental apparatus was designed to carry out the required testing.

The results of the analysis demonstrate the response surface model to be an adequate tool for evaluating and predicting the tested humidifier's performance. The response surface created covers the operational range of the humidifier and can be used as an alternative to one-factor-at-a-time testing. This can be particularly useful at the extremes of the operational range of the humidifier where testing or physical modeling may become challenging due to unstable responses and thermal effects. While the fit of the model lacked some precision on the small scale that cannot be attributed solely to noise, the overall model displayed high accuracy in tracking the results and significance.

The evaluation of the results shows a strong dependence of the humidifier's performance on T_1 . An increase of T_1 leads to a strong negative effect on the humidifier's performance as judged by all metrics. This is mainly attributed to a dehydration of the membrane due to an increased rate of desorption from the membrane. Stream 1 flow rate showed mixed effects on the performance. While an increase in stream 1 flow rate improved the WTR, it simultaneously reduced the efficacy of the humidifier at reaching the desired range of ϕ_2 . The flow rate of stream 3 seemed to have limited influence on the WTR suggesting processes within the membrane to be limiting. The effect of T_3 was found to be mixed as an increase does improve the WTR within the requirement of $\phi_3 = 100\%$ but also demands a greater water transport to increase ϕ_2 .

Acknowledgments

NSERC/MITACS
dPoint Technologies

References

- [1] M.B. Satterfield, P.W. Majsztrik, H. Ota, J.B. Benziger, A.B. Bocarsly, *Journal of Polymer Science, Part B: Polymer Physics* 44 (16) (2006) 2327–2345.
- [2] M.B. Satterfield, J.B. Benziger, *Journal of Physical Chemistry B* 112 (12) (2008) 3693–3704.
- [3] W.R. Merida-Donis, *Diagnosis of PEMFC Stack Failures Via Electrochemical Impedance Spectroscopy*, University of Victoria (Canada), Canada, 2003.
- [4] S.D. Knights, K.M. Colbow, J. St-Pierre, D.P. Wilkinson, *Journal of Power Sources* 127 (1–2) (2004) 127–134.
- [5] M. Watanabe, H. Uchida, Y. Seki, M. Emori, P. Stonehart, *Journal of the Electrochemical Society* 143 (12) (1996) 3847–3852.
- [6] H. Uchida, Y. Ueno, H. Hagihara, M. Watanabe, *Journal of the Electrochemical Society* 150 (1) (2003) A57–A62.
- [7] F.N. Büchi, S. Srinivasan, *Journal of the Electrochemical Society* 144 (8) (1997) 2767–2772.
- [8] F. Liu, B. Yi, D. Xing, J. Yu, Z. Hou, Y. Fu, *Journal of Power Sources* 124 (1) (2003) 81–89.
- [9] M. Watanabe, H. Uchida, M. Emori, *Journal of Physical Chemistry B* 102 (17) (1998) 3129–3137.
- [10] M.V. Williams, H.R. Kunz, J.M. Fenton, *Journal of Power Sources* 135 (1–2) (2004) 122–134.
- [11] R. Huizing, M. Fowler, W. Mérida, J. Dean, *Journal of Power Sources* 180 (1) (2008) 265–275.
- [12] S. Yu, S. Im, S. Kim, J. Hwang, Y. Lee, S. Kang, K. Ahn, *International Journal of Heat and Mass Transfer* 54 (7–8) (2011) 1344–1351.
- [13] D. Kadylak, P. Cave, W. Mérida, *International Journal of Heat and Mass Transfer* 52 (5–6) (2009) 1504–1509.
- [14] D. Chen, W. Li, H. Peng, *Journal of Power Sources* 180 (1) (2008) 461–467.
- [15] H. Bae, K.Y. Ahn, Y.D. Lee, S.K. Kang, S. Yu, *Transactions of the Korean Society of Mechanical Engineers*, B 35 (5) (2011) 473–480.
- [16] S. Park, I.-H. Oh, *Journal of Power Sources* 188 (2) (2009) 498–501.
- [17] S.-K. Park, S.-Y. Choe, S.-H. Choi, *International Journal of Hydrogen Energy* 33 (9) (2008) 2273–2282.
- [18] S.-J. Cheng, J.-M. Miao, S.-J. Wu, *Renewable Energy* 39 (1) (2012) 250–260.
- [19] V.B. Silva, A. Rouboa, *Applied Mathematics and Computation* 218 (12) (2012) 6733–6743.
- [20] W.-L. Yu, S.-J. Wu, S.-W. Shiah, *International Journal of Hydrogen Energy* 35 (20) (2010) 11138–11147.
- [21] W.-L. Yu, S.-J. Wu, S.-W. Shiah, *International Journal of Hydrogen Energy* 33 (9) (2008) 2311–2322.
- [22] J.G. Carton, A.G. Olabi, *Energy* 35 (7) (2010) 2796–2806.
- [23] B. Wahdame, D. Candusso, X. François, F. Harel, J.-M. Kauffmann, G. Coquery, *International Journal of Hydrogen Energy* 34 (2) (2009) 967–980.
- [24] B. Wahdame, D. Candusso, X. François, F. Harel, M.-C. Péra, D. Hissel, J.M. Kauffmann, *IEEE Transactions on Energy Conversion* 23 (4) (2008) 1093–1104.
- [25] R.C. Danté, J.L. Escamilla, V. Madrigal, T. Theuss, J. De Dios Calderón, O. Solorza, R. Rivera, *International Journal of Hydrogen Energy* 28 (3) (2003) 343–348.
- [26] S.-J. Wu, S.-W. Shiah, W.-L. Yu, *Renewable Energy* 34 (1) (2009) 135–144.
- [27] B. Wahdame, D. Candusso, J.-M. Kauffmann, *Journal of Power Sources* 156 (1 Spec. Iss.) (2006) 92–99.
- [28] B. Wahdame, D. Candusso, X. François, F. Harel, A. De Bernardinis, J.-M. Kauffmann, G. Coquery, *Fuel Cells* 7 (1) (2007) 47–62.
- [29] B. Wahdame, D. Candusso, X. François, F. Harel, M.-C. Péra, D. Hissel, J.-M. Kauffmann, Analysis of a Fuel Cell Durability Test Using the Response Surface Methodology, in: *IEEE International Symposium on Industrial Electronics*, vol. 3, 2006, pp. 2007–2012.
- [30] M. Meiler, D. Andre, A. Pérez, O. Schmid, E.P. Hofer, *Journal of Power Sources* 190 (1) (2009) 48–55.
- [31] P. Cave, W. Mérida, *Journal of Power Sources* 175 (1) (2008) 408–418.
- [32] R. Myers, D.C. Montgomery, C.M. Anderson-Cook, *Response Surface Methodology: Process and Product Optimization Using Designed Experiments*, third ed., John Wiley & Sons, Hoboken, NJ, 2009, p. 680.
- [33] D.C. Montgomery, *Design and Analysis of Experiments*, seventh ed., John Wiley & Sons, Inc., Hoboken, NJ, 2009, p. 656.
- [34] J. Larminie, A. Dicks, *Fuel Cell Systems Explained*, second ed., John Wiley & Sons, 2003.
- [35] T. Romero, W. Mérida, *Journal of Membrane Science* 338 (1–2) (2009) 135–144.